J Nanopart Res (2014) 16:2474
DOI 10.1007/s11051-014-2474-3

RESEARCH PAPER

Surface grafting of reduced graphene oxide using nanocrystalline cellulose via click reaction

Roya Kabiri · Hassan Namazi

Received: 14 September 2013 / Accepted: 20 May 2014 / Published online: 12 June 2014

Abstract Reduced graphene oxide (RGO) sheet was functionalized with nanocrystalline cellulose (NCC) via click coupling between azide-functionalized graphene oxide (GO-N_3) and terminal propargyl-functionalized nanocrystalline cellulose (PG-NCC). First, the reactive azide groups were introduced on the surface of GO with azidation of 2-chloroethyl isocyanate-treated graphene oxide (GO-Cl). Then, the resulted compounds were reacted with PG-NCC utilizing copper-catalyzed azide-alkyne cycloaddition. During the click reaction, GO was simultaneously reduced to graphene. The coupling was confirmed by Fourier transform infrared, Raman, DEPT135, and ^{13}C NMR spectroscopy, and the complete exfoliation of graphene in the NCC matrix was confirmed with X-ray diffraction measurement. The degree of functionalization from the gradual mass loss of RGO-NCC suggests that around 23 mass % has been functionalized covalently. The size of both NCC and GO was found to be in nanometric range, which decreased after click reaction.

R. Kabiri · H. Namazi (✉)
Research Laboratory of Dendrimers and Nanopolymers, Faculty of Chemistry, University of Tabriz, P.O. Box: 51666, Tabriz, Iran
e-mail: namazi@tabrizu.ac.ir

H. Namazi
Research Center for Pharmaceutical Nanonotechnology, Tabriz University of Medical Sciences, Tabriz, Iran

Keywords Graphene · Reduced graphene oxide · Nanocrystalline cellulose · Click reaction

Introduction

The incessant progress of nanotechnology in material science has opened new pathways for developing new functional materials. Among them, reduced graphene oxide (RGO) (a one-atom-thick and two-dimension planar monolayer of sp^2-hybridized carbon into a two-dimensional (2D) honeycomb lattice) applications in has great promise for potential many fields (Novoselov et al. 2004; Geim and Novoselov 2007; Erickson et al. 2010) due to its unique chemical, physical, electrical, and mechanical properties (Wang et al. 2009; Xiao et al. 2014). A number of synthetic methods have so far been developed for preparing high-quality graphene (Mao et al. 2011; Kwon et al. 2011). Among them, the chemical reduction of graphene oxide (GO) is considered one of the most promising methods for the large-scale synthesis (Chen et al. 2010; Park and Ruoff 2009). The method includes the steps of oxidation of graphite, dispersion/suspension of oxidized graphite sheets, and reduction of the graphite oxide to graphene. The oxidation introduces the hydroxyl and epoxide groups on the basal planes, as well as the carboxyl and carbonyl groups mostly at the sheet edges of graphene, which increases the hydrophilicity of graphene and the layer distance between GO sheets.

This in turn facilitates the exfoliation and dispersion of GO sheets. The reduction of the dispersed GO to remove the oxygen-containing groups that has been previously introduced in the oxidation step and in order to return the C=C bonds to the molecule, various types of reductants such as hydrazine monohydrate (Tung et al. 2009; Some et al. 2013), NaBH4 (Shin et al.2009), and hydroquinone (Wang et al. 2008) have been used.

Nowadays, research on graphene is a hot topic because of its novel and unique properties such as extremely high carrier mobility, high optical transparency, and superior mechanical flexibility (Novoselov et al. 2012). Graphene-based materials hold strong potential for practical applications in nanoelectronics (Soldano et al. 2013; Brownson et al. 2011), energy-storage (Pumera 2011; Wu et al. 2012), polymer composites (Hwang et al. 2013), liquid crystal devices (Behabtu et al. 2010), and biosensors (Zhu et al. 2012). Moreover, graphene has many biological and medical applications (Cho et al. 2013), which mainly require aqueous stability and biocompatibility. The combination of carbohydrate and GO leads to the formation of hybrid nanostructures with high dispersibility in aqueous media mainly due to the high hydrophilicity of carbohydrates.

Among carbohydrates, cellulose (Siqueira et al. 2010; Namazi and Jafarirad 2008; Namazi et al. 2014) is one of the most widely used biopolymers that exhibits excellent physical properties such as good flexibility, excellent biocompatibility, and biodegradability, and it is also used as insulating component (Moon et al.2011; Yadollahi and Namazi 2013; Namazi et al. 2012). Nanocrystalline cellulose (NCC) is an organic nanomaterial that has recently gained interest as a renewable, environmentally friendly and low cost reinforcing agent for composite materials (Lalia et al. 2013; Abdul Khalil et al. 2012). In addition, it has some appealing intrinsic properties such as high surface area, unique morphology, low density, and high mechanical strength (Habibi et al. 2010). Unlike many nanomaterials, NCC is not synthesized from molecular or atomic components; rather it is obtained by controlled acid hydrolysis of natural cellulose (Bai et al. 2009; Corrêa et al. 2010). The size of nanocrystals depends on the biological origin of cellulose. On the other hand, the use of NCC with exceptionally high mechanical properties instead of microcrystalline cellulose (MCC) can improve the mechanical properties of compounds for the high crystallinity of NCC (Moon et al. 2011; Lavoine et al. 2012; Corrêa et al. 2010).

Scheme 1 Synthesis of click-coupled RGO-NCC: *i* 2-chloroethyl isocyanate, DMF, RT, 24; *ii* NaN_3, DMSO, 50 °C, 48 h; *iii* NaH, LiCl, DMF, 40 °C, 96 h; *iv* $CuSO_4{\cdot}5H_2O$, sodium ascorbate, DMSO, RT, 52 h; and *v* hydrazine monohydrate, 70 °C, 36 h

More recently, some monosaccharides including glucose, fructose, and sucrose were proved to be good stabilizers of graphene in aqueous suspension (Zhu et al. 2010). Furthermore, some polysaccharide molecules were used as both stabilizer and physical cross-linking agents for the preparation of graphene-based multifunctional hydrogels (Shan et al. 2009; Rodríguez-González et al. 2012). Sodium carboxymethyl cellulose/graphene oxide nanocomposite films were fabricated recently (Yadav et al. 2013). The covalent grafting of chitosan (Pham et al. 2010; Bustos-Ramírez et al. 2013) and hydroxypropyl cellulose (Yang et al. 2011) onto the surface of GO has been done by esterification and click reactions (Ryu et al. 2013). The covalent functionalization of RGO with NCC employing click chemistry or other methods has not been reported yet.

NCC is a nontoxic, sustainable, biodegradable, recyclable material, which is produced from abundant renewable resources. The mentioned characteristics for NCC together with its unique mechanical and optical properties have generated a great interest in manufacturing NCC-based products in industrial scale. Therefore, we decided to use NCC for functionalization of RGO. On the other hand, it has been found that the completely protonated acid-form of NCC (H-NCC) is not well dispersible in water once it has been fully dried, even under fairly gentle conditions, while the NCC functionalized with GO has enhanced its dispersibility.

In this study, a stable aqueous suspension of graphene nanosheets fabricated with covalent grafting of NCC on graphene through click reaction. In brief, PG-NCC and GO-N_3 were synthesized. Subsequently, the novel GO-click-NCC was created via the one-step alkyne-azide click reaction in the presence of Cu (I) (Scheme 1). At the end, the dispersed GO-NCC was chemically reduced with hydrazine to obtain a stable aqueous suspension of RGO-NCC.

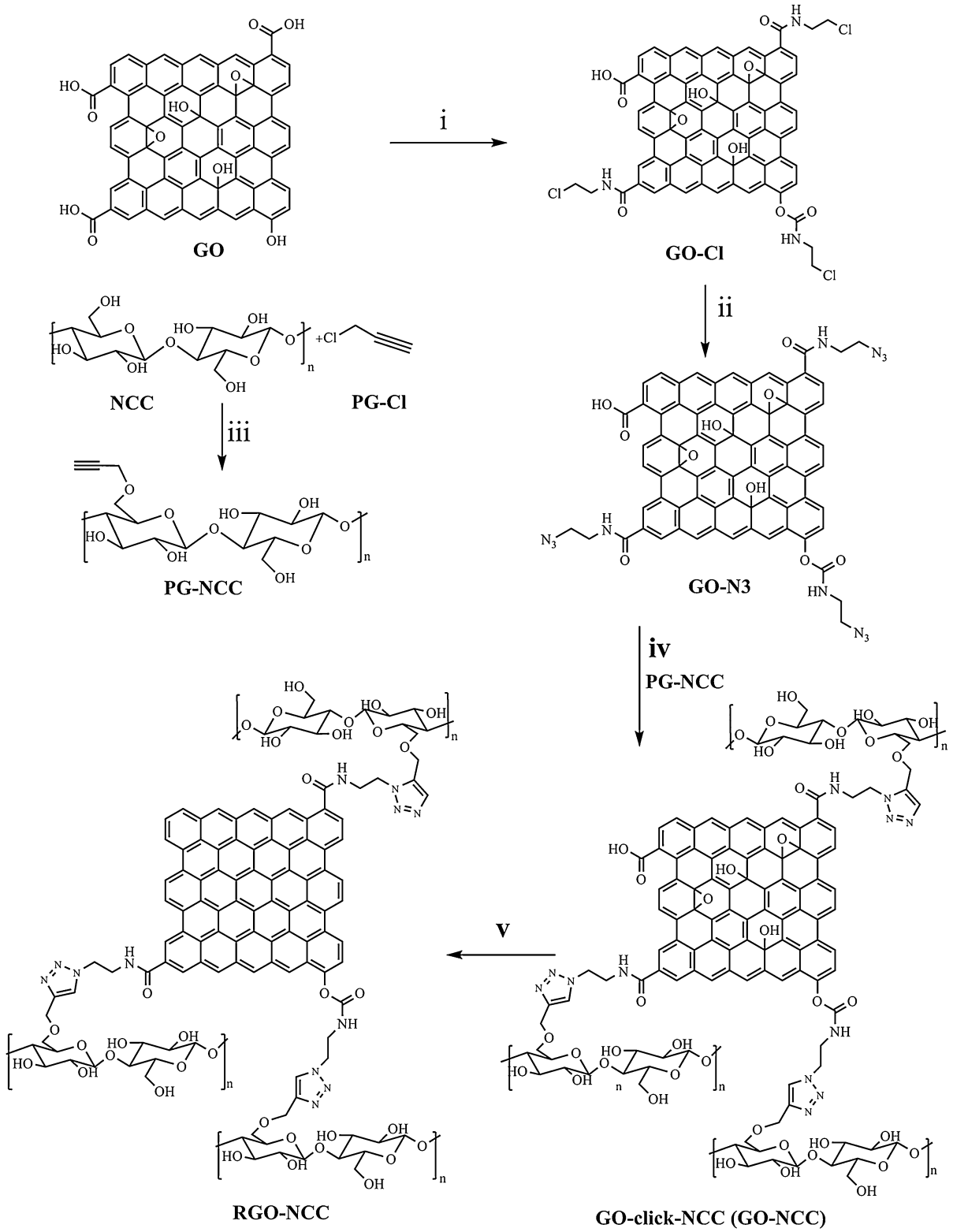
GO
i
GO-Cl
ii
NCC
PG-Cl
iii
PG-NCC
GO-N3
iv
PG-NCC
v
RGO-NCC
GO-click-NCC (GO-NCC)

Materials

Medium molecular weight microcrystalline cellulose (MCC), 2-chloroethyl isocyanate, LiCl, $NaNO_3$, $KMnO_4$, propargyl chloride (PGCl), H_2O_2, H_2SO_4, HCl, methylene chloride, sodium diethyldithiocarbamate trihydrate, and other chemical reagents were obtained from Merck. Sodium ascorbate, copper sulfate pentahydrate, sodium hydride, and sodium azide were purchased from Sigma-Aldrich. Graphite (average particle size 30 μm) is commercially available, which was used without further purification. Dimethyl sulphoxide (DMSO), N,N-Dimethylformamide (DMF), and N, N-dimethylacetamide (DMA) were dried with molecular sieve before use.

Preparation

Preparation of NCC

20 grams of MCC were mixed with the aqueous solution of 64 wt % sulfuric acid (350 ml), and the mixture was stirred vigorously at 45 °C for 3 h. Fivefold dilution was then applied to the mixture to stop the hydrolysis reaction. The suspension was centrifuged to separate the crystals existing in the suspension. The crystals were then washed with distilled water, the mixture was centrifuged, and the crystals were separated again. The process was repeated ten times for each sample. The precipitate was finally placed in regenerated cellulose dialysis tubes (Fisher Scientific, Pittsburgh, PA, USA) having a molecular weight cut-off of 12,000–14,000, and dialyzed against distilled water for several days until the water pH reached a value of 7.0 (Liu et al. 2010).

Preparation PG-NCC

The propargyl cellulose was synthesized by Pai Peng et al.'s method (Peng et al. 2012) with some modification. Briefly, 0.1 g of NCC was stirred in 15 mL DMA at 120 °C for 2 h to allow it swell sufficiently; then 15 % LiCl (w/v) was added. Stirring was continued for 6 h to undertake uniform solubilization. Afterward, the mixture was cooled down to room temperature, followed by the addition of required quantities of NaH (the molar ratio of NaH to anhydrous glucose unit (AGU) was 4:1). After 30 min, the required quantity of propargyl chloride (the molar ratio of propargyl chloride (PG-Cl) to AGU was 10:1) was added slowly under ice cooling. The reaction temperature was kept at 40 °C, and the reaction was run for 96 h. After the required time, the product was precipitated with four volumes of ethanol. The precipitate (color: off-white) was filtered off, and washed with ethanol and distilled water until the pH of the filtrate was neutral. Finally, it was freeze dried.

Preparation of GO

GO was synthesized from the natural graphite powders using a modified Hummers' and Offenman's method (Hummers and Offeman 1958). In brief, 0.5 g of graphite, 0.5 g of $NaNO_3$, and 23 mL of concentrated H_2SO_4 were mixed together and stirred in an ice bath for around 1 h. Then 1.5 g of $KMnO_4$ was added slowly into the solution followed by stirring at 35 °C for 1 day to form thickened paste. Afterward, 23 mL of de-ionized water was added slowly into the solution to avoid the reaction temperature rising to a limit of 98 °C. This solution was then kept stirring for 30 min. Finally, 70 mL of de-ionized water and 5 mL of H_2O_2 (30 %) were poured into the mixture in sequence. This solution was then filtered by gravity filtration, and the filter cake was washed with de-ionized water and 3 % HCl solution alternatively. This filtered cake was then dispersed and washed with de-ionized water for several times by repeated centrifugation. In order to avoid the aggregation of GO in the drying process, the sample was obtained by freeze-drying. Normal drying process produces aggregated GO layers.

Preparation GO-Cl

5 mL of GO in anhydrous DMF (10 mg mL^{-1}) was loaded into a 10-mL round-bottom flask equipped with a magnetic stirring bar. Then organic 2-chloroethyl isocyanate (2 mmol) was added, and the mixture was stirred under nitrogen. After 24 h, the slurry reaction mixture was poured into methylene chloride (50 mL) to coagulate the product. The brown product was then filtered, washed with additional methylene chloride (50 mL), and dried under vacuum (Wang et al. 2012).

Preparation of GO-N_3

To prepare azide-functionalized GO, 6 mmol sodium azide powder was added to 50 mg of GO-Cl dissolved

in 10 ml of post-ultrasonication DMSO (kept in an ice bath to prevent heating) for 10 min. Then the mixture was stirred and refluxed for 48 h at 50 °C in a constant temperature oil bath, thus the azide group was introduced on the GO-Cl sheets via the nucleophile substitution reaction of alkyl halide. Finally, ethyl acetate was used to eliminate any residual DMSO, and the black product was filtered and dried under vacuum.

Preparation of GO-NCC-GO click reaction

The general procedure for azide-alkyne [3 + 2] dipolar cycloaddition to prepare the NCC-click-GO polymer is as follows: after 0.1 g of PG-NNC was dispersed in 10 mL of DMSO, $CuSO_4$-$5H_2O$ (5 mg in 0.5 mL water), sodium ascorbate (10 mg in 0.5 mL water), and GO-N_3 (0.1 g) were added. The mixture was stirred at room temperature for 48 h. 15 mg of sodium diethyldithiocarbamate trihydrate was then added to the mixture to remove the copper catalyst. Isolation took place by precipitation in 400 mL of acetone followed by centrifugation. Then the precipitate was washed with water. The gray product was finally obtained by freeze-drying.

Reduction of GO-NCC to RGO-NCC

RGO-NCC was fabricated by reducing the GO-NCC prepared above. 20 mg of GO-NCC was dispersed in 10 mL of deionized water under sonication for 3 h. Then the resulting yellow exfoliated GO-NCC suspension was reduced with 20 μl hydrazine. The reduction was carried out on a shaker at 400 rpm and 70 °C for 36 h. At the end of the reduction, the RGO-NCC was filtered out from the corresponding suspension and washed twice with water. The dark gray product was finally obtained by freeze-drying.

Characterization and methods

Infrared spectra were obtained on a FTIR spectrometer (Bruker Instruments, model Aquinox 55, Germany) in the 4,000–400 cm^{-1} range at a resolution of 0.5 cm^{-1} as KBr pellets. The carbon nuclear magnetic resonance (^{13}C NMR) and DEPT135 NMR spectra were recorded in DMSO-d_6 in LiCl in 5-mm NMR tubes with a Bruker 100 MHz spectrometer. Raman spectroscopy (Bruker Instruments, model SENTERRA (2009), Germany, Laser wavenumber: 785 nm) was used to confirm the functionalization of GO. The XRD patterns of the samples were obtained by Siemens diffractometer with Cu-ka radiation at 35 kV in the scan range of 2 h from 2 to 70° and scan rate of 1°/min. All of the analyzed samples were in powdery form. Thermo gravimetric analysis (TGA) was performed with a TGA-PL thermal analyzer under air atmosphere from room temperature up to 700 °C at a heating rate of 10 °C/min. Scanning electron micrographs (SEM) were obtained with a LEO 1430VP scanning electron microscope operating at 15 kV. UV–Vis spectroscopy was carried out on a Perkin-Elmer Lambda 35 UV–Vis absorption spectrometer at room temperature. The particle sizes of samples were determined by dynamic light scattering (DLS) using a 90 Plus particle size analyzer equipped with diode laser operating at 658.0 nm. The samples were diluted with distilled water to adjust their solid content to 0.05 wt %, and directly placed in the cell. All measurements were carried out at 25 °C.

Results and discussion

Covalent functionalization of GO with NCC

In a common preparation, GO was synthesized from graphite powder by the Hummers' method. The functional groups containing abundant oxygen make GO sheets vigorously hydrophilic, which improves their solubility in water and provides possibility for more functionalization. As shown in Fig. 6, DLS analysis demonstrated that the average particle size of GO was less than 200 nm. To make use of the Cu-catalyzed Huisgen cycloaddition click reaction, either graphene should contain azide moieties or the second reagent should contain alkynyl moieties (Kolb et al. 2001). In the present study, azide and alkynyl moieties were attached to GO and NCC, respectively (Scheme 1). The azide groups on GO were generated in two steps. Firstly, GO-Cl was prepared by the reaction of GO with 2-chloroethyl isocyanate. The chemical treatment with 2-chloroethyl isocyanate converted hydrophilic functional groups of GO into hydrophobic functional groups, which enabled GO-Cl to be well dispersed in DMSO, DMF, and NMP. In the second step, GO-N_3 was prepared by reacting of GO-Cl with NaN_3. The presence of an absorption azide band in the FT-IR spectra confirmed the presence of an

azide moiety in GO-N_3. ^{13}C NMR analysis was used in order to get more detailed information of the grafted azide on functionalized graphene. Then NCC was prepared through acid hydrolysis of MCC. DLS analysis demonstrated that the average particle size of NCC was in the range of 120–150 nm (Fig. 6). To covalently attach propargyl moieties to the surface of the nanocrystals, we followed the reaction pathway illustrated in Scheme 1. The alkynyl groups on NCC were generated by reaction of NCC and propargyl chloride using NaH in DMA/LiCl. The FT-IR spectrum of PG-NCC indicated the successful incorporation of terminal alkyne groups onto the cellulose chains (two absorption bands at 3,286 and 2,190 cm^{-1}, corresponding to ≡C–H stretching and C≡C stretching, respectively). Finally, the click reaction was conducted at room temperature with $CuSO_4 \cdot 5H_2O$ and sodium ascorbate as the catalyst between alkynyl-functionalized NCC and azidated GO (Scheme 1). Ascorbic acid has been reported as an effective reducing agent for GO that can compete with hydrazine (Fernandez-Merino et al. 2010). Hence, it has an added advantage for click-coupling reactions. FT-IR, ^{13}CNMR, and Raman spectra confirmed a successful coupling reaction as depicted by the five-membered triazole ring with loss of the azide and alkynyl peaks. For the complete reduction of GO in GO-NCC to RGO-NCC, the dispersed GO-NCC was chemically reduced with hydrazine to obtain a stable aqueous suspension of RGO-NCC. This was confirmed by the elimination of GO peaks in the FT-IR spectrum and the red-shift of absorbance peak from 230 to 272 nm in UV–Vis spectroscopy. DLS analysis showed that the average particle size of RGO-NCC was in the range of 70–90 nm (Fig. 6).

FTIR analysis

FT-IR spectra in the 4,000–400 cm^{-1} wave number range in the equal amounts of GO, GO-N_3, NCC, PG-NCC, and GO-NCC are shown in Fig. 1. In the spectrum of GO, the absorbance bands at 1,061, 1,380, 1,620, 1,716, and 3,375 cm^{-1} can be attributed to C–O epoxy, C–O carboxylic acid, C=C aromatic, C=O carboxylic acid, and O–H (broad-coupling hydroxyl group), respectively (Chen et al. 2010). The spectrum of GO-N_3 shows a very broad and intense peak of the O–H group's stretch at about 3,400 cm^{-1}, which is also present in the starting material, and a peak at

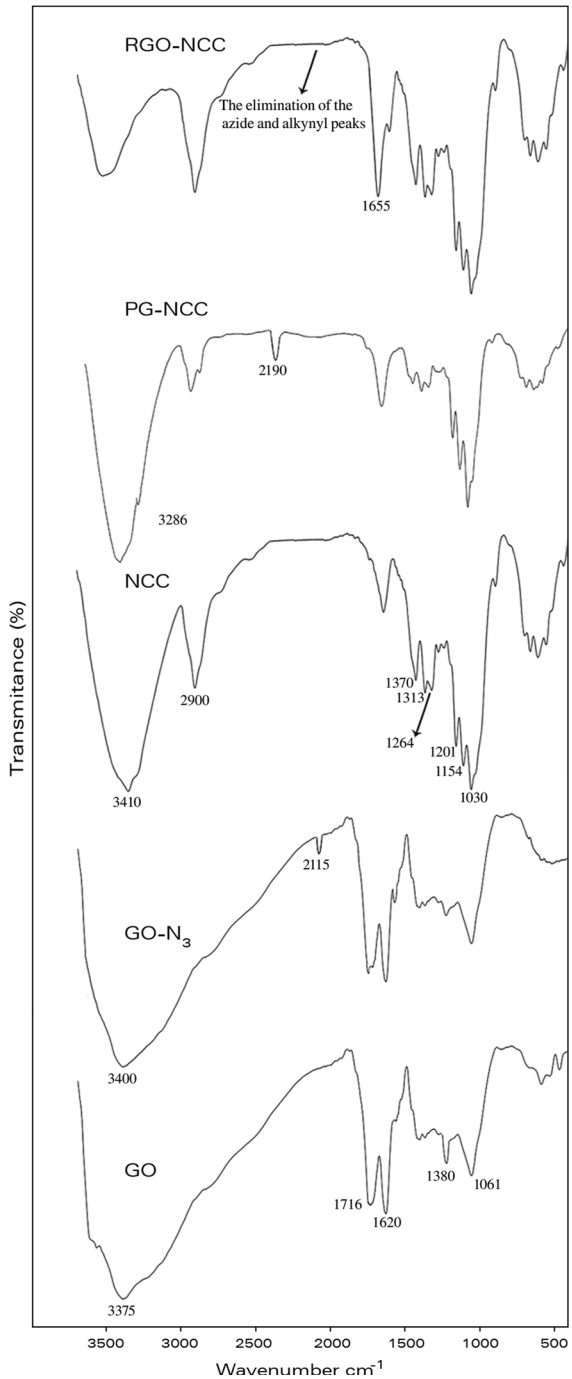

Fig. 1 FTIR spectra of GO, GO-N_3, NCC, PG-NCC, and RGO-NCC

2,115 cm^{-1} that is consistent with the asymmetric stretching of the azide group. The absorbance bands at 3,410, 2,900, 1,370, 1,313, 1,264, 1,201, 1,154, 1,030, and 898 cm^{-1} are associated with NCC (Khan et al.

2012). In the spectrum of PG-NCC, two new absorption bands at 3,286 and 2,190 cm^{-1} (corresponding to ≡C–H stretching and C≡C stretching, respectively) indicate the successful inclusion of terminal alkyne groups onto the cellulose chains. In the spectrum of RGO-NCC, the absorbance band at 1,655 cm^{-1} corresponds to aromatic ring (five-member triazole ring). The elimination of azide and alkynyl peaks shows that the reaction between alkyne groups on the NCC and azide groups on the GO has taken place via click reaction. Furthermore, the intensity of OH group's strength peaks in the RGO-NCC spectrum was decreased (not eliminated because the OH strength of cellulose is located in this area), and CO peaks were eliminated. Which showed that GO has been reduced to RGO during the reaction.

^{13}C NMR analysis

To further verify the occurrence of click reaction, PG-NCC, GO-N_3, and RGO-NCC were investigated by DEPT135 and ^{13}C NMR spectroscopies in DMSO/LiCl by the number scan of 10 k and $d_1 = 20$ s (Fig. 2). In the ^{13}C NMR spectrum of PG-NCC, the signals at 104.5, 76.2–74.3, 65.2, and 59.7 ppm are attributed to the C-1, C3-C-5, C-6, and C-2 of the functionalized glucose units resulting from cellulose, respectively. The signals at 104.8 and 66.7 ppm are attributed to the C-1′ and C-2′ of the unfunctionalized glucose units resulting from cellulose, respectively (Kono et al. 2002; Qi et al. 2009). Other signals of the unfunctionalized glucose units overlap with the functionalized glucose units' peaks. The presence of signals at 82.0, 74.5, and 31.7 ppm is due to the carbons of propargyl groups corresponding to the C-8, C-9, and C-7 of PG-NCC, respectively. In the DEPT135 spectrum of PG-NCC, the resonances of methylene groups (C-7 and C-6) are seen in the reverse phase. The presence of these signals indicates the successful substitution of the propargyl groups on the cellulose chains. In the spectrum of GO-N_3, the peaks at 59, 66, 73, and 78 ppm are attributed to the epoxide, hydroxyl, and two methylene groups, respectively. The resonance at 130 ppm belongs to the un-oxidized sp^2 carbons of the graphene network, and at 155 ppm, it arises from the urethane groups. In the DEPT135 spectrum of GO-N_3, the resonance of methylene groups is seen in the reverse phase. In the spectrum

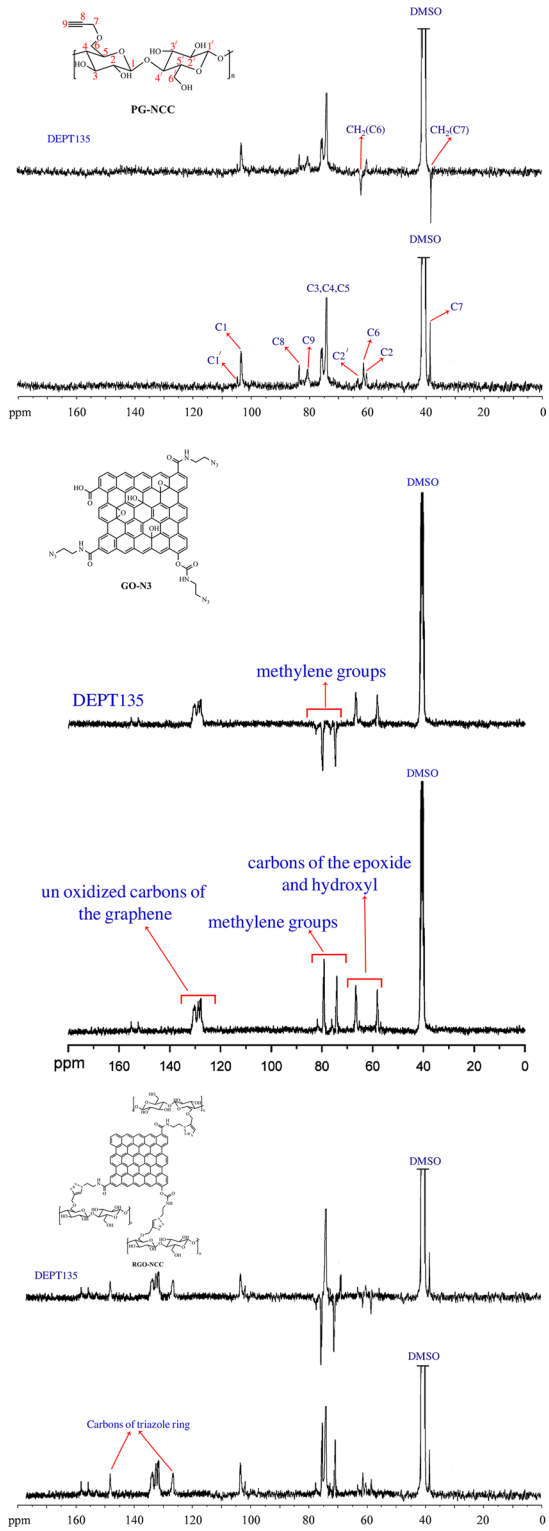

Fig. 2 ^{13}C NMR and DEPT135 NMR of PG-NCC, GO-N_3, and GO-NCC

of RGO-NCC, the presence of signals at 127.4 and 147.1 ppm is attributed to the triazole ring carbons, which supports the successful click reaction between PG-NCC and GO-N3. Moreover, the signals at 38, 61, 77, and 81 ppm are attributed to the methylene groups on RGO-NCC. It was confirmed by DEPT135 analysis results.

Raman analysis

Raman spectroscopy, which is sensitive to the electronic structure, is a valuable tool to study the ordered/disordered crystal structures of carbon-based materials. The known characteristics of Raman spectra for carbon materials are D-band(C–C) and G-band(C=C) that are typically located at about 1,350 and 1,580 cm^{-1} (Stankovich et al. 2007). Figure 3 shows the Raman spectra of GO, GO-NCC, and RGO-NCC. The Raman spectrum of GO, as expected, displays a G peak at 1,585 cm^{-1} corresponding to the first-order scattering of the E2 g mode, and the D band at 1,363 cm^{-1} assigned to the defects introduced upon the oxidation process. The GO-NCC intensity of D-band is increased, supporting the statement that covalent bonding occurs between NCC and GO; this is expected as functionalization results in the increase of sp^3-hybridized sidewall carbons. The Raman spectrum of RGO-NCC also contains both G and D bands; however, there is an increase in the D/G intensity ratio compared to that of GO-NCC. This change suggests a decrease in the average size of the sp^2 domains upon the reduction of the exfoliated GO-NCC, and can be explained that the created RGO-NCC is smaller in size but is higher in number in comparison to GO-NCC.

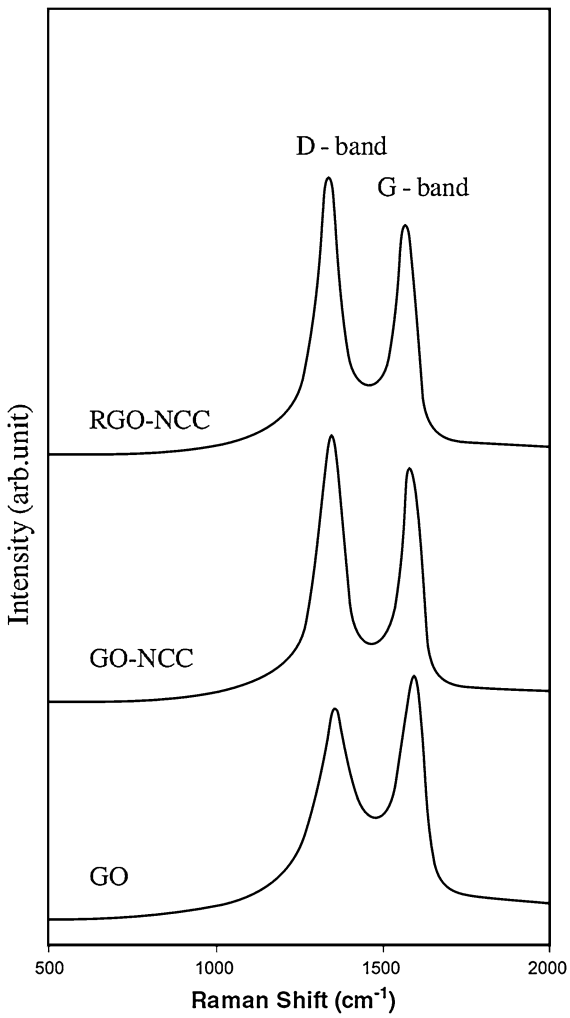

Fig. 3 Raman spectra of GO, GO-NCC and RGO-NCC

UV–Vis analysis

GO, GO-NCC, and RGO-NCC were determined using UV–Vis spectroscopy in aqueous suspension. Figure 4 shows that GO (A) exhibits strong bands centered at 230 and 301 nm, corresponding to the $\pi \rightarrow \pi^*$ transitions of the aromatic C=C band and the $n \rightarrow \pi^*$ transitions of the-COOH band in GO, respectively (Shin et al. 2009). The absorption peak of GO-NCC (B) was red-shifted from 230 to 262 nm. The

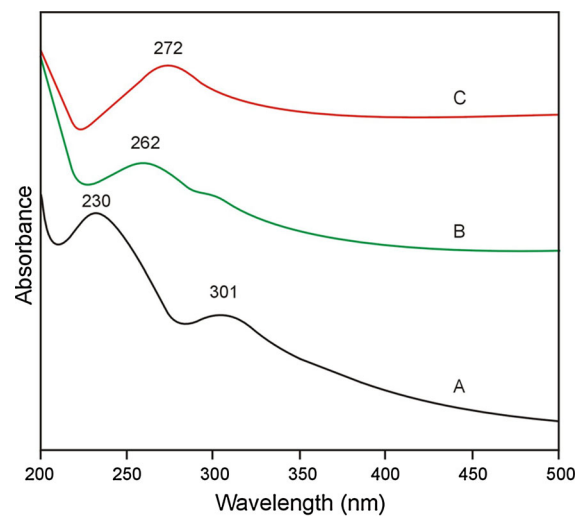

Fig. 4 UV-Vis spectra of *a* GO, *b* GO-NCC, and *c* RGO-NCC

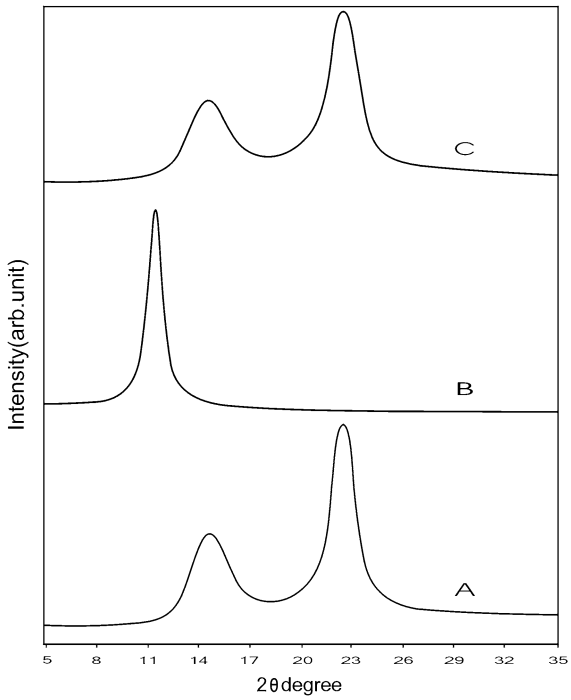

Fig. 5 XRD patterns of *a* NCC, *b* GO and *c* GO-NCC

red-shifted value is smaller than that of fully reduced graphene sheets, which can reach 272 nm, suggesting that GO-NCC was only partially reduced, and its electronic conjugation level is still lower than that of perfect graphene sheets. This partial reduction of GO is probably due to the existence of sodium ascorbate (the salt of ascorbic acid, known as Vitamin C) in the click reaction, which is added originally in order to avoid the oxidization of Cu (I). Vitamin C, as a natural antioxidant, possesses a similar efficiency to hydrazine in the reduction of GO (Fernandez-Merino et al. 2010). The absorption peak of RGO-NCC (C) was red-shifted from 230 to 272 nm; this confirms the reduction of GO-NCC to perfect RGO-NCC.

XRD analysis

NCC, GO, and RGO-NCC were determined using the XRD patterns. The diffractogram of NCC (A) shows the characteristic peaks at $2\theta = 14.8^\circ$ and 22.7° (Shang et al. 2013). The characteristic 2θ peak of GO (B) appearing at 12.1° corresponds to the 001 inter planar spacing of 0.73 nm caused by the oxygen-rich groups on both sides of the sheets and the water

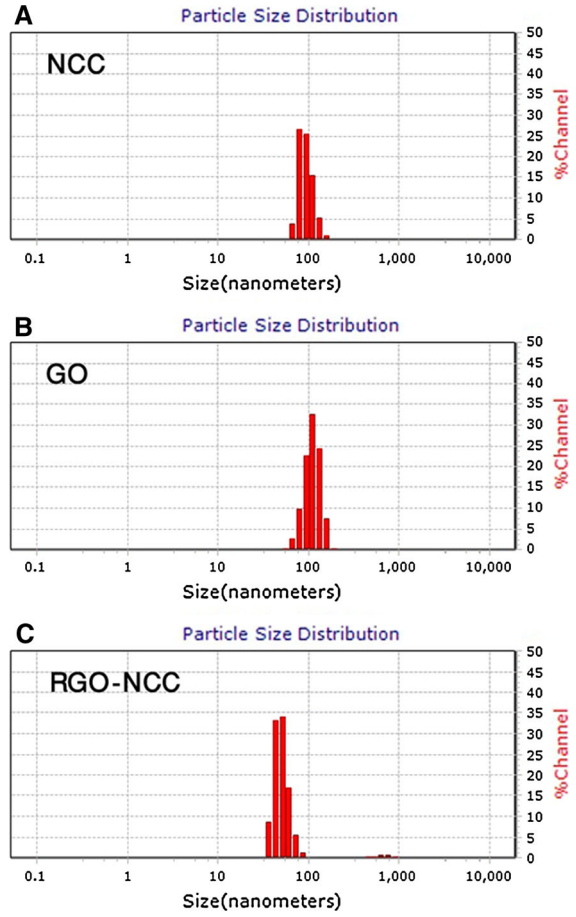

Fig. 6 DLS diagrams of NCC, GO and RGO-NCC

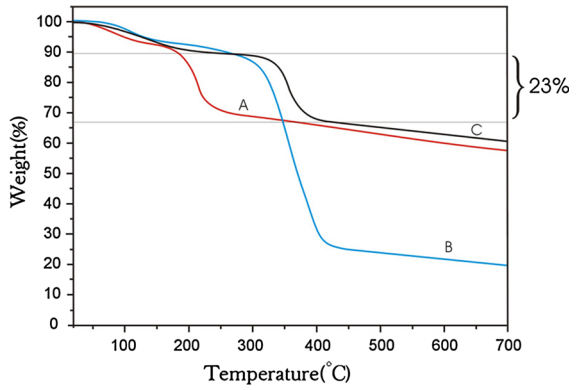

Fig. 7 TGA curves obtained for *a* GO, *b* NCC and *c* RGO-NCC

molecules trapped between the sheets (Ryu et al. 2013). For the GO-NCC (C), the peak at $2\theta = 12.1^\circ$ disappeared, which clearly demonstrates the

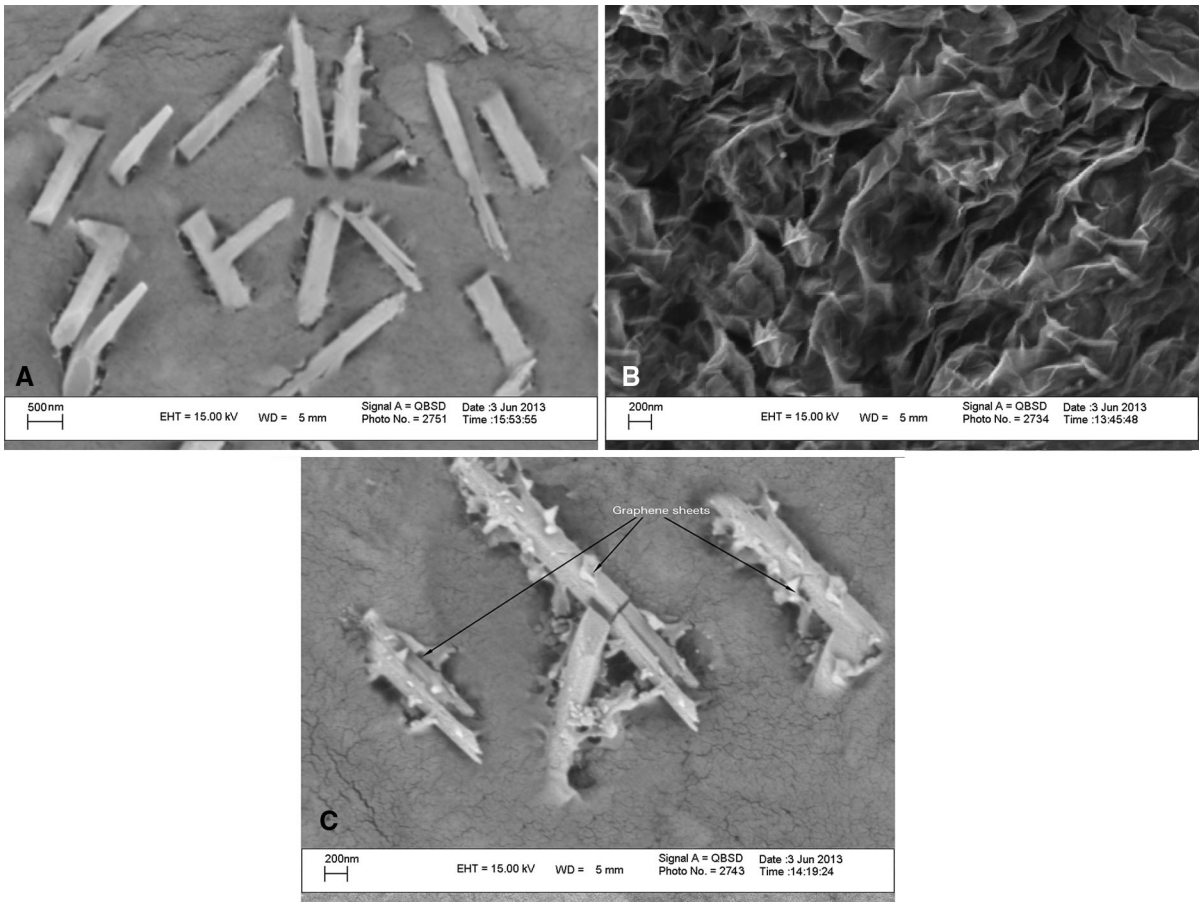

Fig. 8 SEM images of **a** NCC, **b** RGO, and **c** RGO-NCC

formation of a fully exfoliated structure of GO sheets in the polymer matrix and the disappearance of the regular and periodic structure of graphene, whereas the peak at $2\theta = 22.7^{\circ}$ decreased drastically, which can be attributed to the decrease in crystallinity. This suggests that the hydrogen bonding ability of NCC was reduced after the grafting of NCC onto the RGO backbonen (Fig. 5).

DLS analysis

In order to determine the size of NCC, GO, and RGO-NCC, dynamic light scattering (DLS) method was applied in water. The size of NCC and GO was found to be in nanometric range, which was decreased after click reaction. Figure 6 demonstrates that the average particle size of NCC is in the range of 120–150 nm (Lin et al. 2011). After preparation of GO by oxidation of graphite (average particle size 30 μm) and then using sonication, the average hydrodynamic diameters of the graphene oxide sheets were decreased to below 200 nm. The size of RGO-NCC was in the range of 80–90 nm. Reduction in the size of RGO-NCC compared to initial compounds is due to the formation of covalent bonding between RGO and NCC that causes the exfoliation of RGO sheets (Ryu et al. 2013).

Thermogravimetric analysis

The TGA curves of GO (A), NCC (B), and RGO-NCC (C) are shown in Fig. 7. It is apparent that RGO-NCC has different decomposition patterns, compared to pure NCC and GO. GO shows two-step thermal degradation process. The first step can be attributed to the loss of H_2O around 100 °C, and the second step appeared around 225 °C for the loss of acidic

functional groups and residues with total remaining of about 65 %. Above this temperature, GO is almost linearly stable (Moon et al. 2010). The NCC degradation started at slightly lower temperatures and occurred over a wider temperature range of 250–420 °C with the total remaining of about 22 %. It also has only one pyrolysis process (Li et al. 2012). Furthermore, RGO-NCC exhibits no weight loss at 225 °C, suggesting that the oxygen functional groups of RGO are reduced by functionalization. This disappearance of the oxygen functional groups can probably be attributed to their elimination in the functionalization process, as well as to their conversion into more stable triazole rings. The thermal stability of RGO-NCC is higher than that of pure NCC, which can be due to the reduction of GO to RGO. Furthermore, the degree of functionalization from the gradual mass loss of the RGO-NCC suggests that around 23 mass % has been functionalized covalently. It was calculated by the mass loss between 28 and 450 °C over the whole temperature range (Yang et al. 2011; Shen et al. 2010).

SEM analysis

The SEM images of NCC, RGO, and RGO-NCC are shown in Fig. 8 (A-C). The SEM image of NCC films (A) shows a layered pattern of NCC crystallites oriented in a similar direction. The SEM image of RGO (B) consists of randomly aggregated, thin, crumpled sheets closely connected with each other and forming a disordered solid. The SEM image of NCC-RGO (C) shows the successful grafting of RGO on NCC.

Conclusions

As showed, a simple method was developed, involving a three-step reaction pathway, to covalently attachment of NCC molecules onto the surface of GO. Structural details were provided with FTIR spectroscopy, Raman, DEPT135 and ^{13}C NMR spectroscopy. The complete exfoliation of graphene in the NCC matrix was examined using the XRD measurements. The analyses results confirmed a successful coupling reaction as depicted by the five-membered triazole ring. The degree of functionalization from the gradual mass loss of RGO-NCC suggests that around 23 wt % it has been covalently functionalized.

Acknowledgments The authors greatly acknowledge the University of Tabriz and Research Center for Pharmaceutical Nanotechnology (RCPN) for the financial supports of this work.

References

Abdul Khalil H, Bhat A, Ireana Yusra A (2012) Green composites from sustainable cellulose nanofibrils: a review. Carbohydr Polym 87(2):963–979

Bai W, Holbery J, Li K (2009) A technique for production of nanocrystalline cellulose with a narrow size distribution. Cellulose 16(3):455–465

Behabtu N, Lomeda JR, Green MJ, Higginbotham AL, Sinitskii A, Kosynkin DV, Tsentalovich D, Parra-Vasquez ANG, Schmidt J, Kesselman E (2010) Spontaneous high-concentration dispersions and liquid crystals of graphene. Nat Nanotechnol 5(6):406–411

Brownson DA, Kampouris DK, Banks CE (2011) An overview of graphene in energy production and storage applications. J Power Sources 196(11):4873–4885

Bustos-Ramírez K, Martínez-Hernández AL, Martínez-Barrera G, Icaza Md, Castaño VM, Velasco-Santos C (2013) Covalently bonded chitosan on graphene oxide via redox reaction. Materials 6(3):911–926

Chen W, Yan L, Bangal P (2010) Chemical reduction of graphene oxide to graphene by sulfur-containing compounds. J Phys Chem C 114(47):19885–19890

Cho Y, Kim H, Choi Y (2013) A graphene oxide–photosensitizer complex as an enzyme-activatable theranostic agent. Chem Commun 49(12):1202–1204

Corrêa AC, de Morais Teixeira E, Pessan LA, Mattoso LHC (2010) Cellulose nanofibers from curaua fibers. Cellulose 17(6):1183–1192

Erickson K, Erni R, Lee Z, Alem N, Gannett W, Zettl A (2010) Determination of the local chemical structure of graphene oxide and reduced graphene oxide. Adv Mater 22(40):4467–4472

Fernandez-Merino M, Guardia L, Paredes J, Villar-Rodil S, Solis-Fernandez P, Martinez-Alonso A, Tascon J (2010) Vitamin C is an ideal substitute for hydrazine in the reduction of graphene oxide suspensions. J Phys Chem C 114(14):6426–6432

Geim AK, Novoselov KS (2007) The rise of graphene. Nat Mater 6(3):183–191

Habibi Y, Lucia LA, Rojas OJ (2010) Cellulose nanocrystals: chemistry, self-assembly, and applications. Chem Rev 110(6):3479–3500

Hummers WS Jr, Offeman RE (1958) Preparation of graphitic oxide. J Am Chem Soc 80(6):1339

Hwang J, Yoon T, Jin SH, Lee J, Kim TS, Hong SH, Jeon S (2013) Enhanced mechanical properties of graphene/copper nanocomposites using a molecular-level mixing process. Adv Mater 25(46):6724–6729

Khan A, Khan RA, Salmieri S, Le Tien C, Riedl B, Bouchard J, Chauve G, Tan V, Kamal MR, Lacroix M (2012)

Mechanical and barrier properties of nanocrystalline cellulose reinforced chitosan based nanocomposite films. Carbohydr Polym 90(4):1601–1608
Kolb HC, Finn M, Sharpless KB (2001) Click chemistry: diverse chemical function from a few good reactions. Angew Chem Int Ed 40(11):2004–2021
Kono H, Yunoki S, Shikano T, Fujiwara M, Erata T, Takai M (2002) CP/MAS 13C NMR study of cellulose and cellulose derivatives. 1. Complete assignment of the CP/MAS 13C NMR spectrum of the native cellulose. J Am Chem Soc 124(25):7506–7511
Kwon J, Lee SH, Park KH, Seo DH, Lee J, Kong BS, Kang K, Jeon S (2011) Simple preparation of high-quality graphene flakes without oxidation using potassium salts. Small 7(7):864–868
Lalia BS, Samad YA, Hashaikeh R (2013) Nanocrystalline cellulose-reinforced composite mats for lithium-ion batteries: electrochemical and thermomechanical performance. J Solid State Electrochem 17(3):575–581
Lavoine N, Desloges I, Dufresne A, Bras J (2012) Microfibrillated cellulose—Its barrier properties and applications in cellulosic materials: a review. Carbohydr Polym 90(2):735–764
Li W, Yue J, Liu S (2012) Preparation of nanocrystalline cellulose via ultrasound and its reinforcement capability for poly (vinyl alcohol) composites. Ultrason Sonochem 19(3):479–485
Lin N, Huang J, Chang PR, Feng J, Yu J (2011) Surface acetylation of cellulose nanocrystal and its reinforcing function in poly (lactic acid). Carbohydr Polym 83(4):1834–1842
Liu H, Liu D, Yao F, Wu Q (2010) Fabrication and properties of transparent polymethylmethacrylate/cellulose nanocrystals composites. Bioresour Technol 101(14):5685–5692
Mao S, Yu K, Cui S, Bo Z, Lu G, Chen J (2011) A new reducing agent to prepare single-layer, high-quality reduced graphene oxide for device applications. Nanoscale 3(7):2849–2853
Moon IK, Lee J, Ruoff RS, Lee H (2010) Reduced graphene oxide by chemical graphitization. Nat Commun 1:73
Moon RJ, Martini A, Nairn J, Simonsen J, Youngblood J (2011) Cellulose nanomaterials review: structure, properties and nanocomposites. Chem Soc Rev 40(7):3941–3994
Namazi H, Jafarirad S (2008) Preparation of the new derivatives of cellulose and oligomeric species of cellulose containing magneson II chromophore. J Appl Polym Sci 110(6):4034–4039
Namazi H, Fathi F, Heydari A (2012) Nanoparticles based on modified polysaccharides. In: Hashim A (ed) The delivery of nanoparticles. inTech, croatia, pp 149–184
Namazi H, Mosadegh M, Hayasi M (2014) New developments in polycaprolactone-layered silicate nano-biocomposites: fabrication and properties. Handbook of polymer nanocomposites processing performance and application. Springer, New York, pp 21–52
Novoselov KS, Geim AK, Morozov S, Jiang D, Zhang Y, Dubonos S, Grigorieva I, Firsov A (2004) Electric field effect in atomically thin carbon films. Science 306(5696):666–669
Novoselov KS, Fal V, Colombo L, Gellert P, Schwab M, Kim K (2012) A roadmap for graphene. Nature 490(7419):192–200
Park S, Ruoff RS (2009) Chemical methods for the production of graphenes. Nat Nanotechnol 4(4):217–224
Peng P, Cao X, Peng F, Bian J, Xu F, Sun R (2012) Binding cellulose and chitosan via click chemistry: synthesis, characterization, and formation of some hollow tubes. J Polym Sci Part A 50(24):5201–5210
Pham TA, Kumar NA, Jeong YT (2010) Covalent functionalization of graphene oxide with polyglycerol and their use as templates for anchoring magnetic nanoparticles. Synth Met 160(17):2028–2036
Pumera M (2011) Graphene-based nanomaterials for energy storage. Energy Environ Sci 4(3):668–674
Qi H, Liebert T, Meister F, Heinze T (2009) Homogenous carboxymethylation of cellulose in the NaOH/urea aqueous solution. React Funct Polym 69(10):779–784
Rodríguez-González C, Martínez-Hernández AL, Castaño VM, Kharissova OV, Ruoff RS, Velasco-Santos C (2012) Polysaccharide nanocomposites reinforced with graphene oxide and keratin-grafted graphene oxide. Ind Eng Chem Res 51(9):3619–3629
Ryu HJ, Mahapatra SS, Yadav SK, Cho JW (2013) Synthesis of click-coupled graphene sheet with chitosan: effective exfoliation and enhanced properties of their nanocomposites. Eur Polym J 49(9):2627–2634
Shan C, Yang H, Han D, Zhang Q, Ivaska A, Niu L (2009) Water-soluble graphene covalently functionalized by biocompatible poly-L-lysine. Langmuir 25(20):12030–12033
Shang W, Huang J, Luo H, Chang PR, Feng J, Xie G (2013) Hydrophobic modification of cellulose nanocrystal via covalently grafting of castor oil. Cellulose 20(1):179–190
Shen J, Li N, Shi M, Hu Y, Ye M (2010) Covalent synthesis of organophilic chemically functionalized graphene sheets. J Colloid Interface Sci 348(2):377–383
Shin HJ, Kim KK, Benayad A, Yoon SM, Park HK, Jung IS, Jin MH, Jeong HK, Kim JM, Choi JY (2009) Efficient reduction of graphite oxide by sodium borohydride and its effect on electrical conductance. Adv Funct Mater 19(12):1987–1992
Siqueira G, Bras J, Dufresne A (2010) Cellulosic bionanocomposites: a review of preparation, properties and applications. Polymers 2(4):728–765
Soldano C, Talapatra S, Kar S (2013) Carbon nanotubes and graphene nanoribbons: potentials for nanoscale electrical interconnects. Electronics 2(3):280–314
Some S, Kim Y, Yoon Y, Yoo H, Lee S, Park Y, Lee H (2013) High-quality reduced graphene oxide by a dual-function chemical reduction and healing process. Scientific reports 3. doi:10.1038/srep01929
Stankovich S, Dikin DA, Piner RD, Kohlhaas KA, Kleinhammes A, Jia Y, Wu Y, Nguyen ST, Ruoff RS (2007) Synthesis of graphene-based nanosheets via chemical reduction of exfoliated graphite oxide. Carbon 45(7):1558–1565
Tung VC, Allen MJ, Yang Y, Kaner RB (2009) High-throughput solution processing of large-scale graphene. Nat Nanotechnol 4(1):25–29
Wang G, Yang J, Park J, Gou X, Wang B, Liu H, Yao J (2008) Facile synthesis and characterization of graphene nanosheets. J Phys Chem C 112(22):8192–8195
Wang Y, Li Y, Tang L, Lu J, Li J (2009) Application of graphene-modified electrode for selective detection of dopamine. Electrochem Commun 11(4):889–892
Wang Z, Ge Z, Zheng X, Chen N, Peng C, Fan C, Huang Q (2012) Polyvalent DNA–graphene nanosheets "click" conjugates. Nanoscale 4(2):394–399

Wu Z-S, Zhou G, Yin L-C, Ren W, Li F, Cheng H-M (2012) Graphene/metal oxide composite electrode materials for energy storage. Nano Energy 1(1):107–131

Xiao X, Miller PR, Narayan RJ, Brozik SM, Wheeler DR, Brener I, Wang J, Burckel DB, Polsky R (2014) Simultaneous detection of dopamine, ascorbic acid and uric acid at lithographically-defined 3D graphene electrodes. Electroanalysis 26(1):52–56

Yadav M, Rhee K, Jung I, Park S (2013) Eco-friendly synthesis, characterization and properties of a sodium carboxymethyl cellulose/graphene oxide nanocomposite film. Cellulose 20(2):687–698

Yadollahi M, Namazi H (2013) Synthesis and characterization of carboxymethyl cellulose/layered double hydroxide nanocomposites. J Nanopart Res 15(4):1–9

Yang Q, Pan X, Clarke K, Li K (2011) Covalent functionalization of graphene with polysaccharides. Ind Eng Chem Res 51(1):310–317

Zhu C, Guo S, Fang Y, Dong S (2010) Reducing sugar: new functional molecules for the green synthesis of graphene nanosheets. ACS Nano 4(4):2429–2437

Zhu Z, Garcia-Gancedo L, Flewitt AJ, Xie H, Moussy F, Milne WI (2012) A critical review of glucose biosensors based on carbon nanomaterials: carbon nanotubes and graphene. Sensors 12(5):5996–6022